Experimental study of colloidal aggregation in two dimensions. II. Kinetic aspects

D.J. Robinson and J.C. Earnshaw
The Department of Pure and Applied Physics, The Queen's University of Belfast, Belfast BT7 1NN, Northern Ireland
(Received 16 January 1992)

The kinetics of aggregation of colloidal particles at an air-water interface have been investigated. The cluster size distribution and its various moments exhibited scaling with time and cluster size in accord with simulations in which the sticking probability for clusters of size i and j was proportional to $(ij)^{\sigma}$. Modification of the growth conditions caused systematic variation of the scaling exponents, due to changes in the sticking probability exponent σ. The various scaling exponents satisfied a constraint derived from the critical nature of the nonequilibrium aggregation process. Under all experimental conditions the observed kinetics exhibited a crossover from slow to rapid growth, as expected for reaction-limited cluster-cluster aggregation. This implies that the probability of irreversible particle-particle reaction was always very small.

PACS number(s): 68.70.+w, 82.70.Dd, 81.35.+k

I. INTRODUCTION

The aggregation of small particles to form large clusters is a process of fundamental interest in branches of science as diverse as biology, polymer chemistry, atmospheric science, and metallurgy. This practical significance, together with the generally incomplete understanding of the nonequilibrium processes involved, has engendered considerable attention over many years.

There has been a recent resurgence of this interest following discovery of the symmetries associated with the aggregates: the structures exhibit dilational symmetry and are well described in terms of fractal geometry [1]. The characteristic scale invariance of such structures resembles that found for systems at their critical points. There has thus been a hope that an approach to understanding the origin of the fractal nature of the aggregates based on the powerful theoretical techniques developed for studying critical phenomena might prove fruitful [2]. The morphology of the structures is determined by the dominant reaction events, which are also involved in the kinetics of the growth processes. It appears that the kinetics of cluster-cluster aggregation can fall into two distinct regimes, belonging to separate universality classes [3]. The kinetics are most clearly embodied in the cluster size distribution and its time dependence. The shape of this distribution is expected to be universal [4], being independent of the exact nature of the colloidal particles, and governed solely by the aggregation process involved. Thus measurement of the size distribution is crucial both to distinguish the regimes and also to develop a fundamental understanding of the kinetic behavior characterizing them.

A number of models have been proposed to account for the morphology and dynamics of clusters grown in a range of coagulation phenomena. Cluster-cluster aggregation and its several variants are particularly suitable models for the study of multiparticle aggregation encountered in colloidal science [5,6]. Two main variants, diffusion-limited cluster-cluster aggregation (DLCA) and reaction-limited cluster-cluster aggregation (RLCA) have been used, giving rise to rather different cluster morphologies [7, 8]. The structural and kinetic aspects of these phenomena have been investigated in recent large-scale computer simulations of colloidal aggregation, which have yielded significant insight into the processes involved [3, 9–11].

There have been a number of previous experimental studies of the kinetics of aggregation; we mention a few typical examples. Light-scattering studies of various aggregating systems indicated that the cluster size distributions appeared to scale in both size and time [1]. The cluster size distribution of antigens cross linked by antibodies in three-dimensional suspensions was found to be a monotonically decreasing function of the cluster size [12]. However, in coagulation of molecular gases the distributions did not decay monotonically, but rather exhibited a "bell-shaped" form [13]. These differences presumably arise from differences in the aggregation conditions, due to differing particle reaction probabilities. To our knowledge, apart from a preliminary report of the present work [14], there has been only one previous investigation of the kinetics of aggregation in a two-dimensional system, in which scaling laws were demonstrated [15].

Colloidal particles may be spread at a liquid interface to form stable, quasi-two-dimensional monolayers. Our experimental system comprised micrometer-sized colloidal particles trapped on the surface of an aqueous solution [16], aggregation being induced by addition of an electrolyte ($CaCl_2$) solution. In the preceding paper [17] (hereafter referred to as paper I) we have shown that as the electrolyte concentration was increased the morphology of the aggregates suddenly changed, from that characteristic of RLCA to DLCA. Here we consider the corresponding kinetic behavior.

We present measurements of the cluster size distribution and its time dependence, and show that the shape of the distribution is somewhat affected by the aggregation conditions. These results are interpreted in terms of the proposed scaling relations for cluster-cluster aggrega-

tion. The experiment probes the inherent link between the dynamics of aggregation and the resultant structure, a determination of which is essential for a complete understanding of the underlying physics.

II. THEORETICAL BACKGROUND

Various theoretical approaches to the kinetics of aggregation phenomena have been pursued. These include direct analyses based on Smoluchowski's coagulation equation [18, 19], Friedlander's theory of self-preserving spectra [20, 21], and computer simulations [9, 3, 10, 11]. The latter not only directly lead to predictions of scaling characteristics of the cluster size distribution, some of which may also be deduced from the Smoluchowski approach, but also predict morphological characteristics. Here we concentrate upon the results of simulations.

Scaling theory

We briefly summarize the salient features of the scaling phenomena of aggregation kinetics, as revealed by some of the simulations [9, 3, 10].

In "classic" DLCA particles and clusters diffuse at a constant, size-independent rate aggregating irreversibly on first contact (i.e., the probability of reaction is 1). RLCA only differs in that the reaction probability is $\ll 1$, allowing more contacts to be explored before irreversible aggregation occurs. In studies of the kinetics of aggregation these two models have been extended to include a cluster diffusivity or reaction probability which is size dependent [9, 3, 10].

It is assumed that, ignoring shape effects, the diffusion coefficient $\mathcal{D}_s$ scales with the cluster size s as [9]

$$\mathcal{D}_s = \mathcal{D}_0 s^{\gamma}, \tag{1}$$

where $\mathcal{D}_0$ is a constant and γ is the diffusivity exponent. While there are theoretical arguments fixing γ ($\simeq -1/D$, where D is the fractal dimension) in three-dimensional colloidal suspensions [11], the situation is less clear for clusters trapped in two dimensions.

Similarly, the probability that a cluster of size i reacts on contact with a cluster of size j to form a cluster of size $i+j$ may also be size dependent [10]:

$$P_{ij}(\sigma) = P_0 (ij)^{\sigma}, \tag{2}$$

where P_0 is a constant (≤ 1), σ is the sticking probability exponent, and P_{ij} is set to unity if $P_0(ij)^{\sigma} \geq 1$.

The aggregation kinetics fall into two qualitatively different classes, depending on whether γ or σ lies above or below critical values [3, 10]. The critical value γ_c (or σ_c) at which crossover occurs depends upon the space dimensionality d. For $d = 2$, as here, $\gamma_c \sim -0.25$ (for $\sigma = 0$) and $\sigma_c \sim -0.60$ (for $\gamma = 0$). These critical values vary with the magnitude of the other exponent, the effects of the two exponents being similar (and appearing to be additive) [3, 10]. We will call the case where either exponent (or their combination) exceeds the appropriate critical value regime 1, the opposite case being regime 2.

The mass dependences of $\mathcal{D}_s$ and of P_{ij} have similar effects on the form of the cluster size distribution function $n_s(t)$. For $\gamma > \gamma_c$ large clusters are more likely to meet and aggregate. If $\sigma > \sigma_c$ the chance of aggregation occurring when clusters meet is greater when they are larger. Both cases lead to an increased aggregation rate for large s, and thus to a monotonic decrease in $n_s(t)$ with s [3, 10]. Conversely, if either exponent is below its critical value the smaller clusters aggregate faster, so that $n_s(t)$ is no longer monotonic, but becomes bell-shaped with a maximum at a nonzero s [3, 10].

Regime 1. Simulations for $\gamma > \gamma_c$ or $\sigma > \sigma_c$ demonstrate that, in the limit of large t and s and for low particle densities, $n_s(t)$ reduces to a scaling form, which is a function of a single combination of t and s. This regime obviously includes classic DLCA: $\gamma = \sigma = 0$ and $P = 1$. The cluster size distribution can be represented by a form incorporating both dynamic (ω and z) and static (τ) scaling exponents [9]:

$$n_s(t) \propto t^{-\omega} s^{-\tau} h(s/t^z), \tag{3}$$

where the cutoff function $h(x) \sim 1$ for $x \ll 1$ and $h(x) \ll 1$ for $x \gg 1$. The exponents ω, z, and τ are connected by a scaling relation. Assuming that the monolayer density is constant, this scaling form yields [9]

$$\omega = (2 - \tau) z. \tag{4}$$

As ω and z must be positive this implies $\tau < 2$.

Equation (3) leads to characteristic scaling behavior for the total number of clusters and the average cluster size. The weight average cluster size $S(t)$ diverges as

$$S(t) \propto t^z, \tag{5}$$

while the total number of clusters in the system $N(t)$ scales as [9]

$$N(t) \propto \begin{cases} t^{-z}, & \tau < 1 \\ t^{-\omega}, & \tau > 1. \end{cases} \tag{6}$$

The temporal scaling of $N(t)$ thus depends upon the exponent τ, while the exponent for $S(t)$ is always z.

Equation (3) can be written in the alternative form [9]

$$n_s(t) \propto s^{-2} f(s/t^z), \tag{7}$$

with $f(x) \sim x^{\delta}$ for $x \ll 1$ or $f(x) \ll 1$ for $x \gg 1$, where δ is usually called the crossover exponent: $\delta = 2 - \tau$. Thus $n_s(t)$ falls algebraically with s, with exponent τ, up to the cutoff at $x \sim 1$.

Regime 2. In regime 2, where $\gamma < \gamma_c$ (or $\sigma < \sigma_c$), the scaling form [3, 10]

$$n_s(t) \propto s^{-2} \tilde{f}(s/t^z) \tag{8}$$

continues to hold, but with a different cutoff function: $\tilde{f}(x) = x^2 g(x)$ where $g(x) \ll 1$ for $x \ll 1$ and $g(x) \ll 1$ for $x \gg 1$. Thus $\tilde{f}(x)$ goes to zero for *both* small and large x and $n_s(t)$ exhibits a maximum, often described as a bell-shaped curve. There is no τ exponent, as Eq. (3) no longer applies.

Equation (8) can be written as

$$n_s(t) \propto t^{-\omega} g(s/t^z), \tag{9}$$

where $\omega = 2z$ [cf. Eq. (4) with $\tau = 0$]. The scaling laws quoted above for $S(t)$ and $N(t)$ remain valid in regime 2, as they derive from the denominator of x, namely t^z.

Predictions. The form of the scaling function depends on the dynamics of the aggregation process and is different in the two regimes. For $\gamma > \gamma_c$ the cluster size distribution function decays algebraically with s, determined by the static exponent τ, whereas for $\gamma < \gamma_c$ this changes qualitatively, $n_s(t)$ becoming bell-shaped [3, 10].

A common tangent to the cluster size distributions touches $n_s(t)$ in the region where the cutoff behavior of $f(x)$ appears: $x \simeq 1$. Both cutoff functions $f(x)$ and $\tilde{f}(x)$ are about unity at this point. Scaling theory predicts the slope of this common tangent to be -2 in both regimes.

The various scaling laws mentioned above will be examined below. Although the simulations involved very low particle densities it may be hoped that they apply to physically realistic situations. The scaling applies asymptotically, in the limit of large clusters and long times. However, for real systems t is subject to an upper bound because in a system of finite size $N(t)$ eventually becomes so low that $n_s(t)$ loses its meaning, and a crossover to gelation must occur at some time t_g. In this limit the dynamic scaling breaks down.

III. EXPERIMENTAL DETAILS

Most of the experimental procedures have been detailed in paper I, and only a brief summary of the procedures, concentrating on those aspects which are most relevant to the kinetic studies, is required. In the preceding paper we have shown that as the molarity of the aqueous $CaCl_2$ subphase was increased, the fractal structure of the aggregates suddenly changed, from a value compatible with RLCA to one closer to DLCA. The change occurred within the molarity range 0.45–0.55M, and was accompanied by an increase in cluster anisotropy, as expected.

Colloidal particles were spread on the surface of a aqueous solution of 0.001M NaCl, where they were effectively trapped. Such monolayers were stable against aggregation for at least 48 h. Aggregation was induced by "poisoning" the aqueous substrate by injecting $CaCl_2$ solution.

Experimentally all times were measured from the injection of the electrolyte solution. In preliminary experiments [14] a significant change in the kinetics was seen after about 3 h: it was found that the denser $CaCl_2$ solution sank to the bottom of the sample cell on injection, subsequent mixing being governed by diffusion. Various stratagems were adopted to overcome this delayed action, having very similar effects. One example involved gently stirring the subphase (at a rate which avoided shear-induced aggregation) for some 10 min to ensure thorough mixing. Rather surprisingly, as will be seen, these variations in the time for ionic equilibration had very little effect upon the observed aggregation kinetics. We therefore present data taken using all methods.

The concentration of the $CaCl_2$ subphase affects the aggregation process. The higher this concentration, the shorter the Debye screening length of the cloud of counterions surrounding a colloidal particle, the closer the particles can approach, and the greater the chance of sticking on first approach.

The aggregating monolayers were observed microscopically, video images being captured for subsequent analysis. Each pixel was approximately the same size as the 1-μm-diam colloidal particles. The analysis procedures have been detailed in paper I. In analysing the kinetics, as for the structural studies, clusters of 4 or fewer pixels were ignored (see paper I). There was no falloff in resolution as the clusters grow in size.

The area observed was small compared to the whole surface area, ensuring the homogeneity of the sample. The experiments lasted for several hours, during which time slow, gross motions of the surface film meant that different areas were sampled. This does not appear to have affected the results. Typically the area recorded included about 3×10^4 colloidal particles, ensuring rather good statistics in the final results.

IV. RESULTS

The cluster size distribution function is the central quantity of interest in kinetic studies of aggregation. The time dependence of $n_s(t)$ reflects the change of the cluster size distribution during the growth. Our general approach is to consider the gross features of $n_s(t)$, its various scaling behaviors and the collapse of $n_s(t)$ at various times onto common scaling functions for various aggregation conditions.

A. Cluster size distribution

Cluster sizes were defined in terms of the number of pixels comprising the cluster. It is convenient to define $n_s(t)$ as the number of clusters comprising s pixels within the (fixed) surface area observed by the video system. At large sizes there were comparatively few clusters and nonuniform histogram bins are more useful. We use bin widths (δs) which are equal logarithmic increments [usually $\log_{10}(\delta s) = 0.2$] over a range $4 < s < 1000$ pixels.

Figures 1 and 2 show size distributions at various times for two experimental substrate molarities. Typically each data set included over 3×10^4 clusters containing 4×10^5 pixels in total. Generally $n_s(t)$ broadened with time, the number of clusters decreasing and the mass of the largest clusters increasing with time. Initially, and for small times, the distributions tended to exhibit maxima at low s. For substrate molarities $\leq 0.45M$ this maximum persisted and grew into a rather broad peak (Fig. 1). However, above this molarity the distributions evolved to a monotonic decay with s (Fig. 2).

As expected, for the larger molarities $n_s(t)$ could be approximated at large times and below a cutoff value of s by a power law [Eq. (3)]. The cutoff occurred at some characteristic cluster size (whose value increased with time) corresponding to $x \sim 1$ in Eq. (7). Thus after some critical time there were clusters of all sizes up to

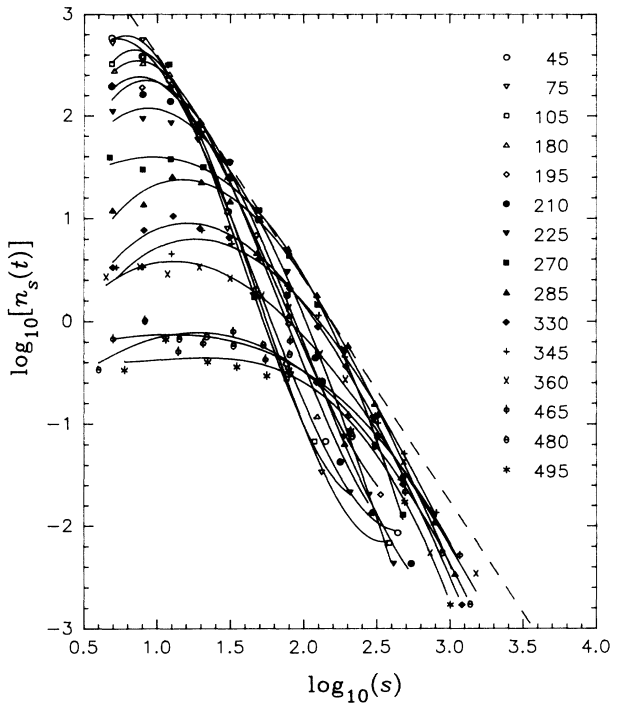

FIG. 1. Cluster size distributions for various times for a $0.25M$ $CaCl_2$ subphase. The legend shows, for each data set, the times (in minutes) from addition of the $CaCl_2$ to the subphase. Here, and in other figures, the lines are spline fits to the data, and only serve to guide the eye. The dashed line indicates the common tangent to the distributions, determined as described in the text.

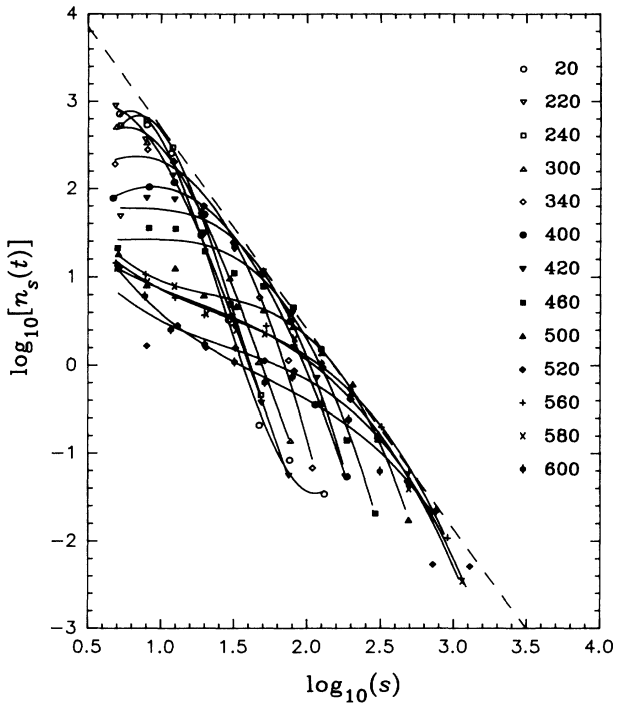

FIG. 2. Same as for Fig. 1, but for a $0.73M$ substrate. The rather different form of $n_s(t)$ from that of Fig. 1 is evident. The static scaling exponent τ was determined from the slopes of the distributions at large t.

a maximum and there was no characteristic cluster size in the system. The absence of a characteristic scale is typical of "critical" behavior.

The scaling regions of $n_s(t)$ observed for all the experiments above $0.45M$ were analyzed to determine the static scaling exponent τ. The data were smoothed using cubic B-spline approximations. For large t, regions of nearly constant gradient (dn_s/ds) were evident below the cutoff. The gradients of such regions were averaged for the different data sets to estimate τ for each experiment (Table I). The values lay in the range $0.4 < \tau < 1.2$, with errors of the order of 30%. As required by Eq. (4), these values are less than 2. Indeed, within the errors τ is < 1, so that $N(t)$ should scale with exponent z [Eq. (6)]. For lower substrate molarities no extended regions of constant gradient were apparent.

Common tangent. One of the most noticeable features of the experimental $n_s(t)$ (Figs. 1 and 2) was that it was possible to draw a common tangent to the curves, in accord with the scaling hypothesis. These common tangents were compared with the predicted slope of -2.0.

The points where the gradient of the spline approximations to the various $n_s(t)$ became -2.0 were identified. They were found to lie close to a straight line (shown dashed in Figs. 1 and 2), giving an indication of the common tangent, of slope m. The values of m (Table I) were largely consistent with the scaling theory prediction, but their absolute values slightly exceeded 2. This discrepancy is probably due to the particle density

TABLE I. Summary of measured static (τ) and dynamic (z, ω) scaling exponents, and gradients (m) of the common tangent. Values of z derived from $S(t)$ and from $N(t)$ are shown separately. Where more than one experiment was carried out for a given concentration weighted averages are quoted.

Conc. $CaCl_2$ (M)	No. expts.	τ	z_S	z_N	ω	$\lvert m\rvert$
0.25	1		4.1 ± 0.5	4.6 ± 0.2	7 ± 11	2.00 ± 0.06
0.360	1		3.5 ± 0.3	3.4 ± 0.4		2.15 ± 0.17
0.45	2		5.5 ± 0.5	6.5 ± 0.6	10 ± 27	2.55 ± 0.24
0.55	1	0.4 ± 0.1	5.6 ± 0.4	5.0 ± 0.3	9.1 ± 6.8	2.08 ± 0.01
0.73	6	0.8 ± 0.1	5.2 ± 0.2	5.5 ± 0.2	5.3 ± 1.6	2.02 ± 0.02
0.91	1	1.2 ± 0.3	7.8 ± 0.8	9.3 ± 1.6	11 ± 16	2.16 ± 0.16

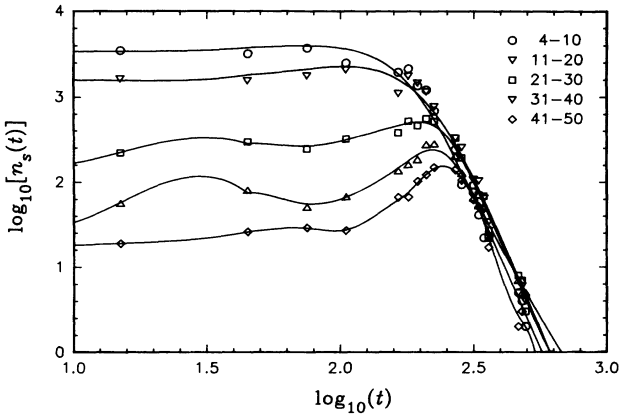

FIG. 3. Plot of $\log_{10}[n_s(t)]$ vs $\log_{10}(t)$ for data from Fig. 1. The legend shows the cluster size ranges corresponding to each data set. The dynamic exponent ω was determined from the asymptotic scaling regions.

and finite size of our experimental system which make eventual gelation inevitable. Very large clusters would be more likely to intersect the boundary of the video image than small ones (and thus be rejected—see paper I), so that the image analyzed will be artificially deficient in large clusters. Thus at large times $n_s(t)$ would tend to be reduced somewhat at large s, increasing the gradient of the common tangent. While statistical corrections for these effects could be applied, the existence of common tangents to the present experimental data and their slopes provide strong support for the scaling hypothesis

Dynamic scaling of $n_s(t)$. Figure 3 shows a typical set of distributions $n_s(t)$ plotted as a function of time for several different ranges of cluster size. The general behavior is as expected from the simulations. The number of small clusters fell monotonically as they joined together to form larger clusters. However, the initial population of intermediate size clusters (all but the smallest class shown) was negligible, so that $n_s(t)$ first grew, only decreasing later as these clusters aggregated to form larger clusters. In the limit of large times the numbers of clusters of all sizes except the very largest must fall.

At large times scaling behavior was evident. Power-law fits to each curve in these asymptotic limits yielded the dynamic scaling exponent ω. By averaging these values the exponent was estimated for each experiment (Table I). In one experiment ($0.36M$) no extended region of scaling could be found. At $0.73M$ no significant differences could be found in the fitted values of ω for experiments in which the onset of rapid aggregation was delayed. This suggests that this aspect of the scaling behavior was not materially affected by the different times for ionic equilibration noted above.

B. Scaling of N(t) and S(t)

The variations with time of the total number of clusters $N(t)$ and the weight average cluster size $S(t)$ were investigated. Two typical sets of data are shown in Fig. 4, plotted on the same scale to enable direct comparisons to be made between experiments.

The scaling was often evident only over a rather narrow range of time because of various effects.

(i) Initially $S(t)$ grew slowly, but at large t it increased more rapidly, apparently as a power law in time. This will be discussed fully below.

(ii) In some experiments the mean cluster size $S(t)$ saturated at long times due to the finite size of the system.

(iii) The effect of the initially monodisperse distribution may have taken some time to decay.

Variations in the protocol used in adding $CaCl_2$ to the subphase did not, as originally expected [14], lead to variations in z (Fig. 5). In certain experiments time delays due to ionic equilibration were eliminated, but rapid cluster growth still did not occur from $t = 0$. Once rapid aggregation set in, the average cluster size grew at a rate essentially independent of the delays, but dependent on the substrate molarity, confirming the lack of effect of the different times for ionic equilibration upon the scaling behavior.

Given the limited time span of the scaling regime, it was difficult to positively identify the behavior of $S(t)$ as power law or exponential. The data of Figs. 4 and 5 are replotted semilogarithmically in Figs. 6 and 7 to enable the reader to form some idea of the likely applicability of exponential growth. We found that power-law fits were

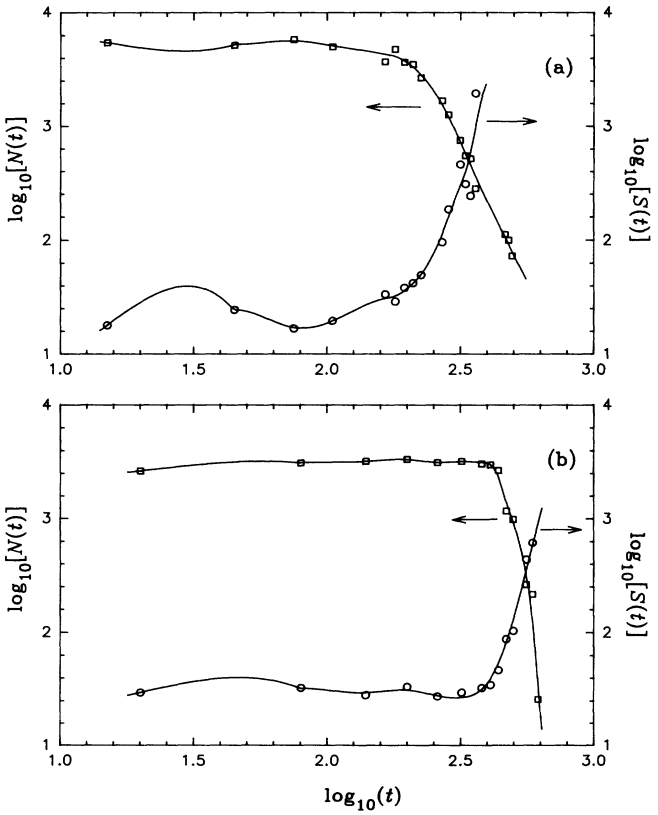

FIG. 4. Plot of $\log_{10}[S(t)]$ and $\log_{10}[N(t)]$ for experiments on (a) $0.25M$ and (b) $0.91M$ $CaCl_2$ subphases. The dynamic exponent z was estimated from the slopes of the asymptotic scaling regimes for both quantities.

usually better than those involving an exponential function. The values of the exponent (z_S) obtained by the power-law fits to $S(t)$ in the asymptotic region are given in Table I. The fitted exponents were about 5, tending to rise with increasing molarity. Such large exponents were difficult to measure accurately. The experimental reproducibility is indicated by the spread of the results for the several $0.73M$ experiments: from 4.4 ± 0.5 to 6.5 ± 0.4. However, it is clear that the increase of $S(t)$ is more rapid at $0.91M$ than at $0.25M$ (Fig. 4).

The rate of disappearance of clusters is related to the rate of increase of the average cluster size. The time dependence of $N(t)$ is ultimately determined by the static scaling exponent τ [Eq. (3)]. Only if τ is less than 1.0 will the dynamic scaling of the $S(t)$ and $N(t)$ data be the same. In fact, power-law fits to the asymptotic behavior of $N(t)$ yielded values of the exponent (z_N) which corresponded quite well with those from $S(t)$ (Table I). This provides an independent check upon the values of τ given above.

C. Collapse onto common form

A further check of the scaling of $n_s(t)$ is possible. Equations (7) and (9) can both be written in the form

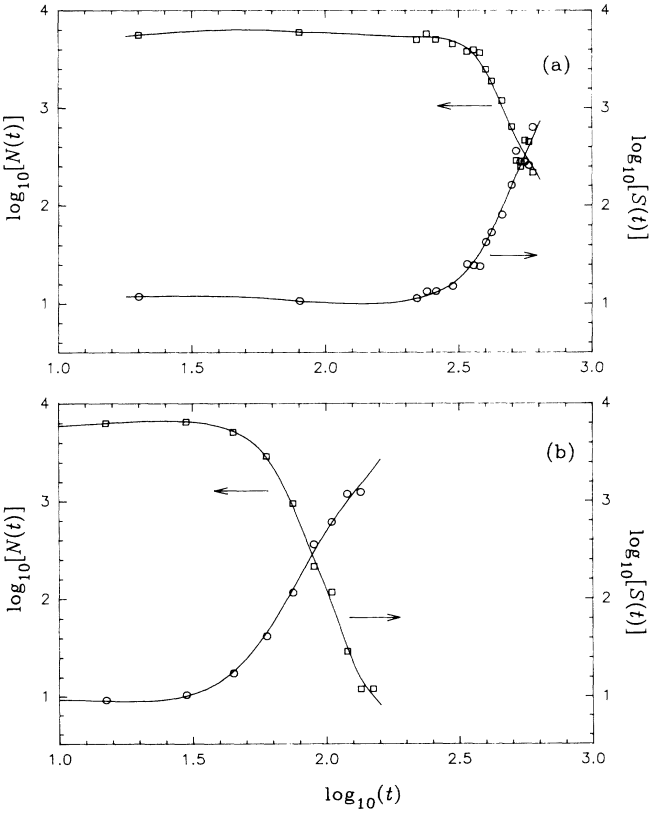

FIG. 5. Comparison of the variations of $\log_{10}[S(t)]$ and $\log_{10}[N(t)]$ for two experiments on $0.73M$ subphases. In (a) the $CaCl_2$ was allowed to mix by diffusion, whereas in (b) the subphase was stirred (see text). The z exponents were very similar in both cases: e.g., $z_S = 5.8 \pm 0.5$ for (a) and 4.9 ± 0.4 for (b), despite rapid aggregation being delayed to 320 min in (a) compared to 30 min in (b).

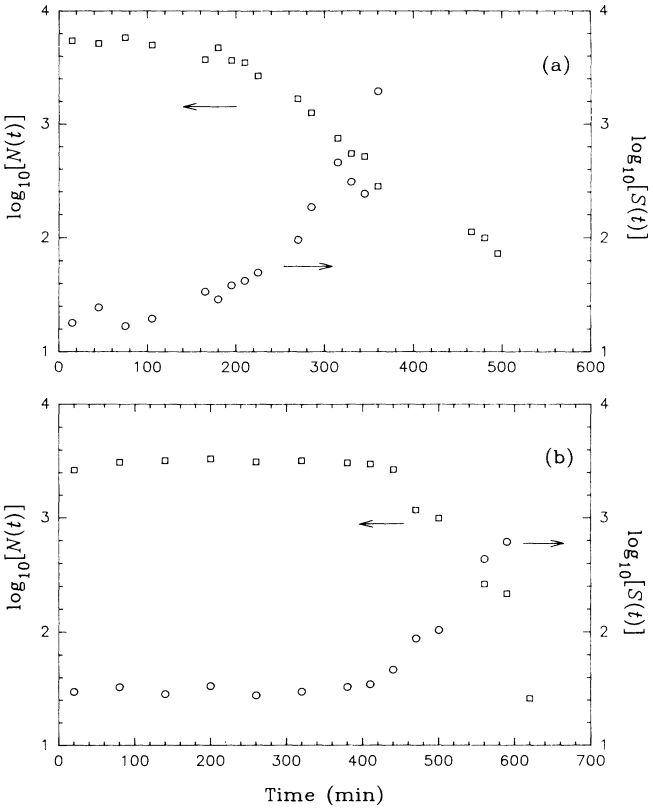

FIG. 6. The data of Fig. 4 replotted against time, to enable the reader to compare the likelihood of exponential growth kinetics, as opposed to the power-law behavior of that figure.

$$n_s(t) \propto t^{-2z} F(s/t^z), \tag{10}$$

where $F(x)$ is $f(x)/x^2$ in regime 1 or $g(x)$ in regime 2. Recalling that $S(t) \propto t^z$, this suggests that when, for a given experiment, $S^2(t)n_s(t)$ is plotted against $s/S(t)$ the distributions for all times should collapse onto a common functional form, different for the two scaling regimes. The data at both short and long times may not collapse correctly on to the common form: at small t due to the delay in the onset of scaling of $S(t)$ (cf. Fig. 5), and at large t because of statistical fluctuations of $n_s(t)$.

Now in regime 1, $f(x) \sim x^\delta$ for $x \ll 1$ or $f(x) \ll 1$ for $x \gg 1$, whereas in regime 2, $g(x) \ll 1$ for both $x \ll 1$ and $x \gg 1$. Very different forms of $F(x)$ in Eq. (10) are thus expected in the two regimes. In regime 1, recalling that $\delta = 2 - \tau$, $F(x) \propto x^{-\tau}$ below $x = 1$, falling very rapidly above $x = 1$. In regime 2, however, $F(x)$ is just $g(x)$ and thus exhibits a peak at $x = 1$.

For all experiments $n_s(t)$ was replotted in the form expected. Two representative cases are shown in Figs. 8 and 9. The reduction of the distributions for each experiment to a unique master curve is quite evident, apart from certain departures at small t, probably due to the cause just noted. The cluster size distribution can indeed be described by $N_s(t) \sim t^{-2z} F(s/t^z)$, the shape of the master curves reflecting the intrinsic properties of the aggregation process. The forms of $F(x)$ are almost ex-

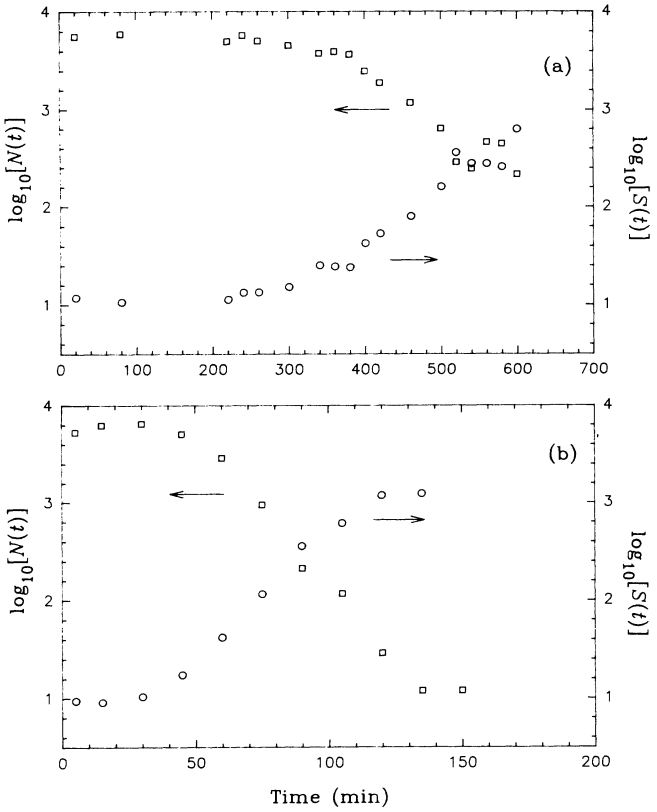

FIG. 7. The data of Fig. 5 replotted semilogarithmically, to illustrate the possibility of exponential kinetics.

actly the same for the two examples shown, except that the lower molarity data show a rather flatter function for $x < 1$. Similar effects were observed for all experiments. The reduction to a common scaling function does not involve any adjustable parameters, and provides a further check on the scaling hypothesis.

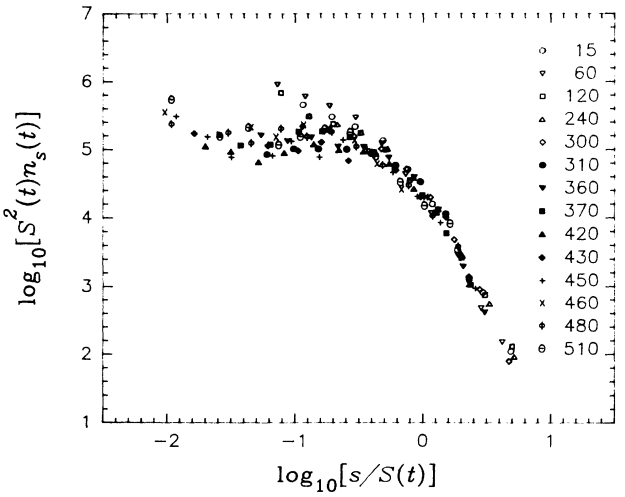

FIG. 8. The observed $n_s(t)$ for an experiment on a $0.36M$ subphase, scaled to a common form. The legend shows the times (in minutes) from addition of the $CaCl_2$ to the subphase for each data set. Apart from the small s data at the three lowest times, the collapse of the distributions onto a single function is excellent.

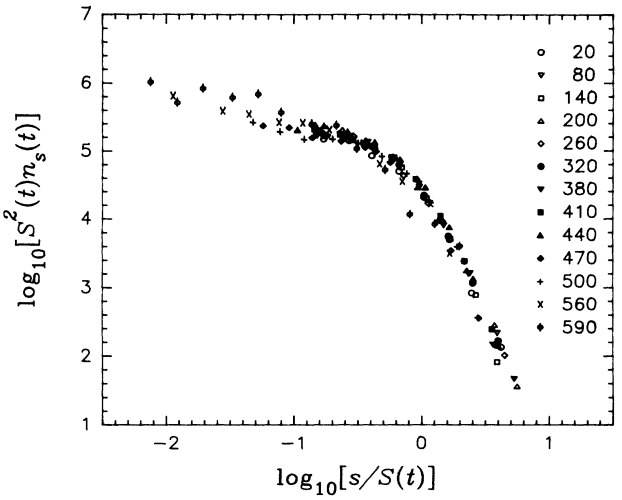

FIG. 9. Same as for Fig. 8, but for an experiment on a $0.91M$ subphase [same data as Fig. 4(b)]. The data set at the largest time is omitted as it was very noisy. The common form onto which the data collapse differs somewhat from that at low subphase molarity; see text.

V. DISCUSSION

We have examined the evolution of the cluster size distribution function of latex particles aggregating in two dimensions. Morphologically the clusters observed at long times in these experiments appear to conform to expectations for RLCA and DLCA in two dimensions (paper I). The change between the two structural regimes occurred at substrate concentrations between $0.45M$ and $0.55M$. We may ask whether there is a change in kinetics associated with this change in structure.

In comparing the present experimental results with the scaling theory, the existence of two scaling regimes must be borne in mind. To recap, these correspond to values of the diffusivity exponent (γ) or the sticking probability exponent (σ) which exceed, or are less than, critical values.

Physically $\mathcal{D}_s$ would be expected to fall as the cluster mass increases: $\gamma < 0$. However, visual inspection of our colloidal monolayers clearly showed that the larger clusters were more mobile. We do *not* associate this mobility with Brownian motion: simply stated, larger clusters tended to move about more rapidly than smaller ones. The reasons are not clear, but it may be that the large clusters confined on a liquid interface are more susceptible to residual thermal air currents, present despite the sample cell being enclosed. At all events the physical phenomena seem to affect the aggregation process in a manner similar to that corresponding to $\gamma > 0$ (i.e., above γ_c). While the diffusion coefficient cannot rise with cluster mass, it is convenient to speak of an "effective" γ which is positive. There seems no physical reason why

this effective γ should depend upon the concentration of the $CaCl_2$ subphase, whereas this will affect σ. We conclude that any variations of the observed phenomena with substrate molarity probably reflect the effects of σ. The effects due to σ appear to be partially offset by those due to the positive effective γ [10]. In fact, some appropriate combination of γ and σ must be considered, as the effects of the two exponents seem to be additive [10]. In the absence of any more definite information, $(\gamma+\sigma)$ will be used as shorthand for this combination, without any implication that this is correct.

Figure 3 is consistent with a positive effective γ. The population of small clusters ($s \leq 20$) decays rather slowly at first because of the infrequent collision rate and small sticking probability for these small clusters, but after a certain period, when some larger clusters have formed, the decrease becomes very rapid. It would appear that smaller clusters disappear rapidly because of aggregation with the more mobile larger clusters, rather than with other small clusters.

The cluster size distributions observed broadly agree with the expected forms [3]. The existence of common tangents to the size distributions and the closeness of the gradients to the predicted value support the scaling hypothesis.

At the higher subphase molarities $n_s(t)$ decays algebraically with s (Fig. 2). This indicates that $(\gamma + \sigma)$ exceeds the appropriate critical value. Given that the effective $\gamma > 0$, we can only say that σ cannot be so small that the combined exponent falls below this critical value. The values of the static scaling exponent τ determined for substrate molarities $\geq 0.55M$ (Table I) were compatible with $(\gamma + \sigma)$ being above the critical value.

The value of the τ exponent is clearly dependent upon the concentration of the $CaCl_2$ subphase. As we believe the effective γ is constant, this implies that the sticking probability exponent σ increases systematically with subphase concentration. This conclusion is supported by other aspects of the results.

At lower $CaCl_2$ concentrations ($\leq 0.45M$) $n_s(t)$ took a rather different form, exhibiting a broad maximum at nonzero s for at least some intermediate times (Fig. 1). In these experiments it was not possible to find extended regions of scaling with s, and so τ could not be determined. Both these features suggest that $(\gamma+\sigma)$ fell below the critical value. Simulations suggest that in this case $n_s(t)$ will adopt a bell-shaped form [3, 10]. There is a tendency towards this behavior at low salt molarity, but the expected large maxima in the experimental cluster size distributions were never clearly observed. In particular the common form found on collapse of the size distribution functions (Figs. 8 and 9) never displayed a marked peak, as expected when $(\gamma + \sigma) < (\gamma + \sigma)_c$ [Eq. (9)].

In all our data, maxima in the $n_s(t)$ apparently only occurred during the transition to the asymptotic behavior. Overall the common forms onto which collapse occurred were compatible with $(\gamma + \sigma) > (\gamma + \sigma)_c$ (i.e., scaling regime 1) with $\tau \geq 0$ at all substrate molarities: i.e., $f(x)/x^2 \propto x^{-\tau}$. The master functions were, indeed, compatible within error with the fitted values of τ, including $\tau = 0$ for subphase concentrations $\leq 0.45M$. This suggests that under all conditions $(\gamma + \sigma)$ never fell significantly below its critical value. Under appropriate conditions it appears, however, that bell-shaped size distributions can be observed in two-dimensional colloidal aggregation [22], presumably due to different conditions.

The common forms found by collapse of $n_s(t)$ for different substrate molarities (Figs. 8 and 9) only differed for $x \leq -0.5$, indicating the validity of the scaling arguments. It is remarkable that the common function found by collapse of data from the only other study [15] of which we are aware agreed excellently with that from the present data for $x > -0.5$. That study involved aggregation of 3.6-μm magnetized spheres; differences at low values of x would be expected if the static exponent τ differed for the two systems due to differences of γ or σ. The agreement of the scaling functions for two systems involving such different interparticle interactions provides powerful evidence for the universality of the scaling theory [2, 4].

Taken together the above results provide the strongest evidence that the present data obey the scaling hypothesis, the static exponent τ being in good agreement with expectations, while the common tangent and rescaled distributions include certain dynamic aspects of the scaling. The collapse of the size distributions assumes algebraic scaling of $S(t)$, and the success of this procedure indicates the correctness of this assumption.

Other dynamic scaling phenomena were also in broad accord with expectation from the simulations. Asymptotically $n_s(t)$, $S(t)$, and $N(t)$ appeared to scale algebraically with t. In simulations [3, 10] it has proved impossible to distinguish between algebraic scaling, exponential scaling and a gelation transition: $S(t) \propto (t_g - t)^{\alpha}$. It was similarly difficult to distinguish algebraic and exponential scaling in the present experimental data. Power-law fits to the data seemed somewhat better, although the differences were probably not statistically significant. For comparison with the simulations it is, however, convenient to concentrate on the algebraic scaling.

The data for $n_s(t)$, $N(t)$, and $S(t)$ yielded the dynamic exponents ω and z for various values of the sticking probability exponent σ (γ being essentially fixed). The exponents were determined from the sometimes rather limited asymptotic regions of the data and are therefore subject to relatively large uncertainties. In the asymptotic regime the z exponent from both $S(t)$ and $N(t)$ increased systematically with the substrate molarity (Fig. 10). Given the apparent constancy of the effective γ, this affords further evidence of the effective modification of σ by the substrate molarity.

The values reported here for the dynamic exponents far exceed those from the computer simulations underpinning the scaling theory [9, 3, 10]. The simulations are only expected to be strictly valid in the zero density limit, as they deal with considerably lower initial concentrations than can realistically be attained experimentally ($\sim 8\%$ surface coverage). However, this cannot explain the finite time delay before rapid aggregation occurred for the

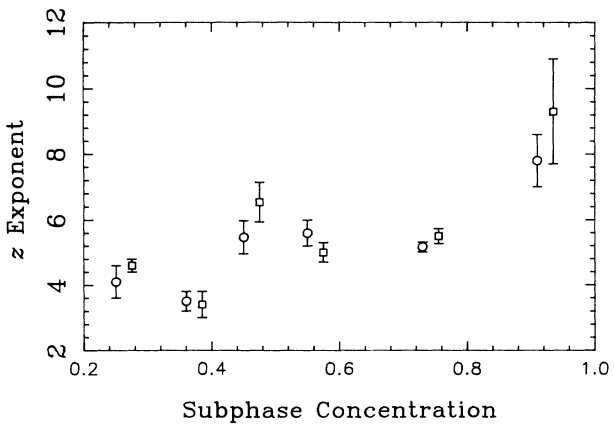

FIG. 10. The variation of the dynamic scaling exponent determined from both $S(t)$ [z_S (○)] and from $N(t)$ [z_N (□)] with molarity of the $CaCl_2$ solution. The z_N data are displaced horizontally for clarity.

experiments.

The present results still serve as a physical test of the validity of any theoretical treatment. We have sought asymptotic scaling behavior: while the exponents may not be strictly correct their relative values may still have some merit. They may well be affected by processes not taken into account in the simulations cited. Despite the large uncertainties, the absolute values of the static (τ) and dynamic (ω and z) exponents are consistent with the relationship $\omega = (2-\tau)z$ [Eq. (4)] expected from simulations. For all our experimental data the combination $[\omega-(2-\tau)z]$ was compatible with zero within the errors. The best test uses the $0.73M$ $CaCl_2$ data, for which the weighted mean was -1.1 ± 1.7.

The unexpected aspects of the aggregation behavior, primarily the delayed onset of the dynamic scaling behavior and the consequent large values of the exponents, could arise from a crossover from RLCA to DLCA. They are not a function of diffusive delays in ionic equilibration of the subphase, and must be due to the underlying aggregation mechanism. At small t there are only small clusters in the system. If they do not stick on collision, there is a good chance that they separate again. The number of clusters thus decreases slowly—the aggregation is reaction limited. As t increases, larger clusters appear which can make contact at many points, the sticking probability becomes essentially unity, and the process crosses over into DLCA. The question of this delayed onset of aggregation and its possible origin is discussed fully in the following paper [23].

Simulations of RLCA have indeed shown that a crossover in the kinetics to DLCA does occur [10, 11]. Initially $S(t)$ and $N(t)$ change very slowly, only approaching their asymptotic algebraic scaling (with exponent z) after times which depend upon the particle-particle sticking probability P_0 [10]. More recent simulations, albeit in three dimensions, using rather different dependences of sticking probability on cluster size than that of Eq. (2) suggest that the exponent z may be very high, ≥ 4 [11]. The present results may well afford quantitative support to this picture. We do not pursue this here because different formulations used for P_{ij} in these simulations lead to some differences in the predicted exponents [11].

Such a crossover may explain the variations of the shape of $n_s(t)$ at the lower molarities (Fig. 1), where σ is apparently smallest. In these experiments the maxima in $n_s(t)$ began to develop during the RLCA phase of aggregation, but were apparently suppressed as the crossover to DLCA took place. At the higher subphase molarities, where σ is larger, the tendency for $n_s(t)$ to develop into a bell-shaped curve will be less as $(\gamma+\sigma)$ will be further from the critical value, so that this feature of the crossover behavior would be less evident.

Returning to the comparison with the structural studies of paper I, the change in structural character from RLCA to DLCA at subphase concentrations between $0.45M$ and $0.55M$ does not seem to be accompanied by a marked change in aggregation kinetics. Instead we find only a subtle variation in the kinetic behavior (see following paper [23]). All the observed aggregation kinetics may be explained by the combined effects of a constant, positive effective cluster diffusion exponent and an experimentally variable cluster sticking probability exponent.

VI. CONCLUSIONS

We have studied the kinetics of colloidal aggregation in two dimensions. The experimental results agree with the hypothesis that this process obeys scaling laws. The results, over a wide range of experimental conditions, are entirely self-consistent, and in quantitative accord with the results of recent simulations [9, 3, 10, 11]. Comparisons with other experimental data [15] support the idea that the process is universal in character.

The salt in the aqueous subphase decreased the range of the repulsive part of the interparticle interactions, and hence increased the interparticle sticking probability. Whereas increasing the salt concentration leads to an abrupt change in the structure of the aggregates, no such change is apparent in the kinetic aspects. At low subphase molarities the structures accord with expectation for RLCA, while at high values they agree with DLCA (paper I). However, the effect on the kinetics of increasing the subphase concentration seemed to be more gradual and continuous. This effect resembled that which would be expected from certain computer simulations [10] if the rate at which the sticking probability varies with cluster size were to increase systematically with salt concentration.

The dynamic scaling found here suggests that at all subphase concentrations a crossover occurs from RLCA to DLCA-like phenomena as the aggregation proceeds. This appears to contradict the structural studies (paper I) which reveal rather sharp concentration dependent changes in morphology. It is thus clear that a simple determination of the fractal dimension of an aggregating system cannot, of itself, provide conclusive evidence concerning the nature of the aggregation process involved. The complete picture is much more complex, and cannot be described by a single parameter. There is, indeed,

some apparent difficulty in reconciling the structural and kinetic aspects of the present study. The following paper [23] deals with the time dependence of the morphology of the aggregates and demonstrates that these difficulties can be resolved.

ACKNOWLEDGMENTS

This work was supported by the SERC. One of us (D.J.R.) gratefully acknowledges financial support from DENI and Unilever Research.

[1] P. Meakin, in *Phase Transitions and Critical Phenomena*, edited by C. Domb and J.L. Lebowitz (Academic, New York, 1988), Vol. 12, p. 335.
[2] A.A. Lushnikov, J. Colloid Interface Sci. **45**, 549 (1973).
[3] P. Meakin, T. Vicsek, and F. Family, Phys. Rev. B **31**, 564 (1985).
[4] M.Y. Lin, H.M. Lindsay, D.A. Weitz, R.C. Ball, R. Klein, and P. Meakin, Proc. R. Soc. London Ser. A **423**, 71 (1989).
[5] P. Meakin, Phys. Rev. Lett. **51**, 1119 (1983).
[6] M. Kolb, R. Botet, and R. Jullien, Phys. Rev. Lett. **51**, 1123 (1983).
[7] R. Botet, R. Jullien, and M. Kolb, J. Phys. A **17**, L75 (1984).
[8] M. Kolb and R. Jullien, J. Phys. (Paris) **45**, L977 (1984).
[9] T. Vicsek and F. Family, Phys. Rev. Lett. **52**, 1669 (1984).
[10] F. Family, P. Meakin, and T. Vicsek, J. Chem. Phys. **83**, 4144 (1985).
[11] P. Meakin and F. Family, Phys. Rev. A **38**, 2110 (1988).
[12] G.K. von Schulthess, G.B. Benedek, and R.W. De Blois, Macromolecules **13**, 939 (1980).
[13] K. Sattler, in *Advances in Solid State Physics*, edited by P. Grosse (Vieweg, Braunschweig, 1983), Vol. XXIII, p. 1.
[14] J.C Earnshaw and D.J. Robinson, Prog. Colloid Polym. Sci. **79**, 162 (1989).
[15] G. Helgesen, A.T. Skjeltorp, P.M. Mors, R. Botet, and R. Jullien, Phys. Rev. Lett. **61**, 1736 (1988).
[16] P. Pieranski, Phys. Rev. Lett. **45**, 569 (1980).
[17] D.J. Robinson and J.C. Earnshaw, preceding paper, Phys. Rev. A **46**, 2045 (1992).
[18] P.G.J. van Dongen and M.H. Ernst, Phys. Rev. Lett. **54**, 1396 (1985).
[19] R.C. Ball, D.A. Weitz, T.A. Witten, and F. Leyvraz, Phys. Rev. Lett. **58**, 274 (1987).
[20] S.K. Friedlander and C.S. Wang, J. Colloid Interface Sci. **22**, 126 (1966).
[21] F.S. Lai, S.K. Friedlander, J. Pich, and G.M. Hidy, J. Colloid Interface Sci. **39**, 395 (1972).
[22] A.J. Hurd and D.W. Schaefer, Phys. Rev. Lett. **54**, 1043 (1985).
[23] D.J. Robinson and J.C. Earnshaw, following paper, Phys. Rev. A **46**, 2065 (1992).